Nonlinear Optics at Excited States of Exciton Polaritons in Two-Dimensional Atomic Crystals

Xiaoze Liu,[#] Jun Yi,[#] Quanwei Li,[#] Sui Yang, Wei Bao, Chad Ropp, Shoufeng Lan, Yuan Wang, and Xiang Zhang*

Cite This: https://dx.doi.org/10.1021/acs.nanolett.9b04811

Read Online

ACCESS | 📊 Metrics & More | 📖 Article Recommendations | 🆂🆈 Supporting Information

ABSTRACT: Exciton polaritons (EPs) are partial-light partial-matter quasiparticles in semiconductors demonstrating striking quantum phenomena such as Bose−Einstein condensation and single-photon nonlinearity. In these phenomena, the governing process is the EP relaxation into the ground states upon excitation, where various mechanisms are extensively investigated with thermodynamic limits. However, the relaxation process becomes drastically different and could significantly advance the understanding of EP dynamics for these quantum phenomena, when excited states of EPs are involved. Here, for the first time, we observe nonlinear optical responses at the EP excited states in a monolayer tungsten disulfide (WS_2) microcavity, including dark excited states and dynamically metastable upper polariton bands. The nonlinear optics leads to unique emissions of ground states with prominent valley degree of freedom (DOF) via an anomalous relaxation process, which is applicable to a wide range of semiconductors from monolayer transition metal dichalcogenides (TMDs) to emerging halide perovskites. This work promises possible approaches to challenging experiments such as valley polariton condensation. Moreover, it also constructs a valley-dependent solid-state three-level system for terahertz photonics and stimulated Raman adiabatic passage.

KEYWORDS: *Nonlinear optics, exciton polaritons, monolayer transition metal dichalcogenide, excited states, relaxation dynamics*
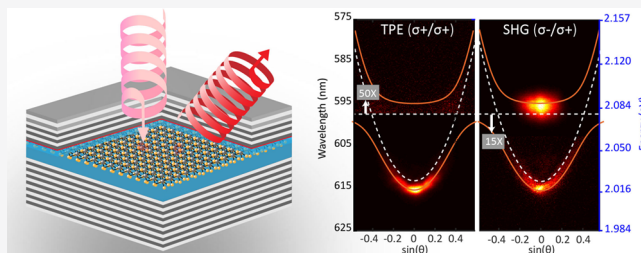
Exciton polaritons (EPs) are the fundamental solid-state quasiparticles in the framework of cavity quantum electrodynamics (QED).[1,2] They are the coherent superposition of excitons and photons in semiconductor cavities under the strong coupling regime, where the coupling rate is faster than the average dissipation rate of excitons and cavity photons.[1] EPs demonstrate remarkable physical phenomena such as Bose−Einstein condensation (BEC) and single-photon nonlinearity, which are extremely difficult in solid-state materials.[1,2] These phenomena are all determined by the EP relaxation dynamics to ground states (lowest polariton band) once they are excited, involving various competing mechanisms with the thermalization process.[1,2] Depending on the relaxation efficiency, the final population distribution of EPs with respect to the ground states could enable various exotic quantum properties for polariton condensation and nonlinear optics.[1,2] However, distinct relaxation dynamics would be introduced to develop the conventional understanding of key processes for EP physical phenomena, when EP excited states (higher energy bands) are involved. These excited states introduce unique fundamental properties, such as different parity symmetry and quantum coherence,[1−8] leading to abundant QED with distinct light−matter interactions, including coherent energy exchange,[3,4] ultrafast terahertz transitions,[5,6] and optical selection rules.[5,6,8−10]

Here we for the first time observe nonlinear optics at EP excited states in a monolayer tungsten disulfide (WS_2) microcavity, leading to unique emissions of ground states with prominent valley degree of freedom (DOF) via the anomalous relaxation process. The nonlinear optical responses originating from the excitonic resonances in monolayer WS_2 grant the optical access to these excited states of EPs in the WS_2 microcavity. They also unravel the physical properties of EP excited states and track down the relaxation dynamics with valley DOF, introducing unconventional relaxation processes with excited states to overcome the thermalization limits in the linear optical excitation scheme.[11,12] This first observation not only promises great possibility with nonlinear optical approaches to challenging landmark experiments such as valley BEC and chiral superfluids[12,13] but also demonstrates a unique three-level system[6] with valley DOF for terahertz photonics and stimulated Raman adiabatic passage (STIRAP) in the solid-state platform.[14]
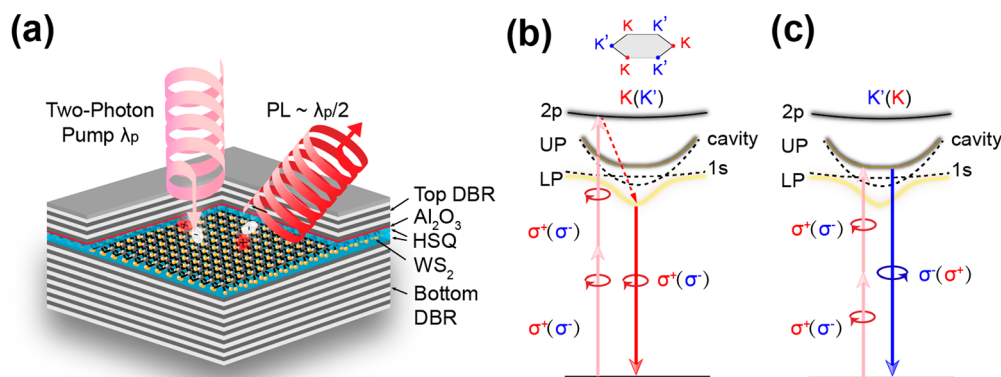
Figure 1. Schematics of sample structure and energy diagram of valley exciton polariton (EP) quantum states. (a) The microcavity (MC) sample structure consists of bottom and top distributed Bragg reflectors (DBRs) and a cavity composite layer where a monolayer of WS_2 is sandwiched between two hydrogen silsesquioxane (HSQ) layers as well as a protection layer of Al_2O_3. The nonlinear spectroscopy approach is via excitation with a normal incident two-photon pump and detecting signals at angular far field. (b) The energy diagram of valley EP. In the strong coupling regime, valley EPs are formed with two degenerate sets labeled as K (red) and K′ (blue), originated from the 2D excitons (as the inset of the hexagonal Brillouin zone). In each set, the exciton 1s states (dashed line) couple with cavity photon modes (dashed curve), leading to two bands of lower polariton (LP, solid orange curve) and upper polariton (UP, solid gray curve). The excitonic dark 2p states (solid black curve) can be accessed by two-photon photoluminescence excitation (TPE). The lowest band LP is taken as the ground state, while the bands of UP and dark 2p states refer to excited states. They could quickly relax to the LP and emit circularly polarized photons by considering the direct transition channel between them. (c) The polariton-resonant second-harmonic generation (SHG) for probing UP. When SHG is taken as an instantaneous process, SHG emits out through UP states with the opposite helicity of pump photons due to the angular-momentum conservation.

The nonlinear optical responses at these excited states of WS_2 EPs include two-photon photoluminescence excitation (TPE) and second-harmonic generation (SHG) spectroscopy through the underlying optical selection rule. EPs discovered lately in monolayer transition metal dichalcogenides (TMDs) offer a novel testbed to explore the EP quantum states with valley DOF.[11,12,15−17] TMD monolayers are an attractive group of direct-gap two-dimensional (2D) semiconductors to host excitons,[18,19] with large binding energy (up to ∼0.7 eV),[20,21] huge oscillator strengths,[18,20] and new valley DOF.[22−24] By placing the 2D excitons in cavities, robust EPs can be formed at room temperature[15,25,26] and strikingly have been found to be equipped with valley DOF.[25−28] The 2D TMD EPs offer three outstanding advantages. First, the large exciton binding energy facilitates the spectroscopic identification of quantum states of 2D EPs;[9,21,29] second, the valley DOF provides a unique quantum mark to monitor these states;[22−27] third, the broken inversion symmetry in TMD monolayers results in strong SHG signals acting as an instantaneous process to probe metastable states.[9,29]

An all-dielectric microcavity (MC) embedded with mono-layer WS_2 (Figure 1a) is studied for our demonstration. The MC consists of a bottom mirror (15.5 pairs of Nb_2O_5/SiO_2 distributed Bragg reflector (DBR)), a top mirror (7.5 pairs of Si_3N_4/SiO_2 DBR), and a cavity composite layer. The composite layer includes an exfoliated monolayer WS_2, two sandwiching layers of hydrogen silsesquioxane (HSQ), and a capping layer of Al_2O_3.[30] The nonlinear spectroscopy is carried out by two-photon pump and far-field detection of polarization-resolved emission. The sample preparation and optical experiments are elaborated in the Experimental Methods.

The energy diagram and experimental approach of nonlinear optics are outlined in the schematic of Figure 1b and c. The optical transitions of K(K′) valley excitons in monolayer WS_2 can be enabled by left (right) circularly polarized $\sigma^+(\sigma^-)$ photons with optical spin $m_{ph} = 1$ ($m_{ph} = -1$). When valley excitons are strongly coupled to a planar MC, the EPs lead to

two degenerate sets of energy bands labeled as K and K′[25−28] (Figure 1b). In each set, the excitonic 1s states couple to cavity photons and form two anticrossed bands of upper polariton (UP) and lower polariton (LP) as the coherent superposition of excitons and cavity photons. For example, UP states can be described as $|UP_{K(K')}\rangle = \alpha|ex\_1s_{K(K')}\rangle + \beta|photon\rangle$, where α, β are the Hopfield coefficients for the superposition and vice versa for the LP states (see Analysis). The UPs are optically active but thermodynamically unstable; thus, they would quickly decay to LP states based on the thermodynamic relaxation.[3] For the parity symmetry, the excitonic 2p states cannot couple with one photon but can only relax to lower energy states, acting as another higher dark energy band.[5,6,9,21,31] For the energy levels and the correlations among them, the lowest band LP is taken as the EP ground state, while the dark 2p states and the UPs are two typical kinds of EP excited states[6] which are difficult to be probed in conventional linear optics. The experimental approach of nonlinear optics is based on TPE of dark 2p states (Figure 1b) and resonant SHG with the dynamically unstable UPs (Figure 1c). Note here that the nonlinear optical responses are all much stronger than the isolated monolayer WS_2 without a cavity (see Figure S8 in the Supporting Information), and the enhanced nonlinear optics would better probe the EP excited states in the cavity.

The dark 2p states can be excited by TPE from the electronic ground state g_e (not polariton ground-state LP) with a rate of $W^{2ph(\omega)}_{g_e \to 2p}$. Following relaxation $W_{2p \to LP}$ from 2p to LP, the TPE can induce LP fluorescence with a decay rate of $W^{ph(\sim 2\omega)}_{LP \to g_e}$ and an intensity as[32,33]

$$I_{TPE} \propto W^{2ph(\omega)}_{g_e \to 2p} W_{2p \to LP} W^{ph(\sim 2\omega)}_{LP \to g_e} \tag{1}$$

Through these three processes, the total angular momentum should be conserved for resonant excitation of 2p states with circular polarization. By only considering the valley DOF without depolarization from the intervalley scattering, TPE
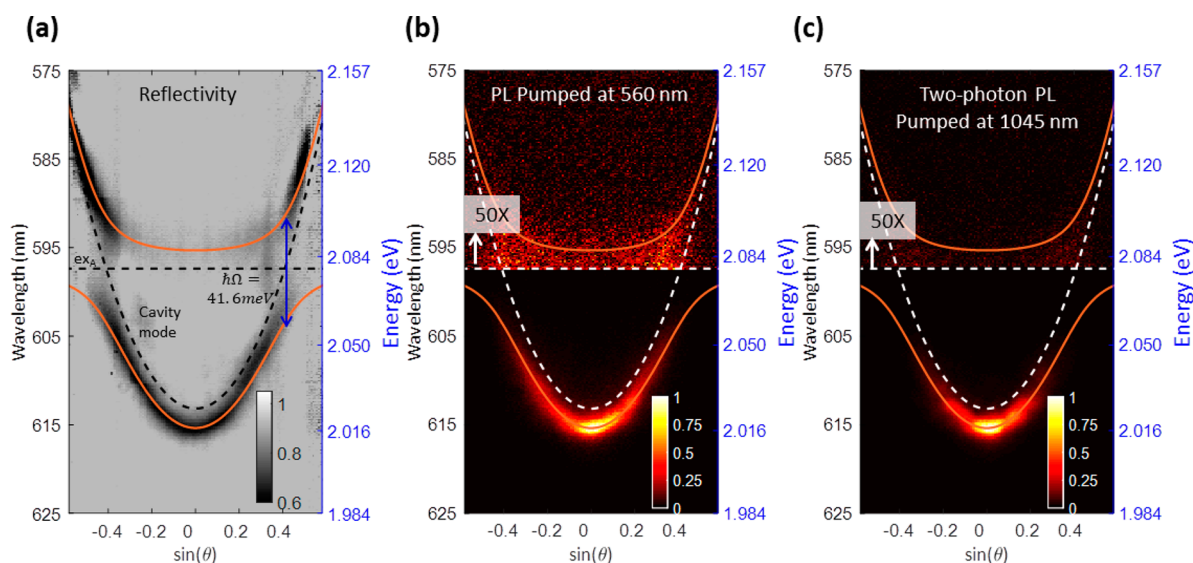
Figure 2. Determination of the strong coupling regime via k-space reflectivity and photoluminescence (PL) at 80 K. (a), The k-space (angle-resolved) reflectivity map with photon energy versus sine of angles (θ). The reflectivity modes are revealed at dark areas of the map. Two polariton branches are identified by anticrossing dispersion with a 41.6 meV Rabi splitting in a coupled oscillator model, where the dashed line represents the exciton A 1s states (ex$_A$) at 2.075 eV and the dashed curve represents the cavity photon mode. The gray color scale represents the reflectivity. The k-space PL maps by (b) nonresonant linear pump at 560 nm and (c) TPE pump at 1045 nm. This TPE pump corresponds to a resonance of the dark 2p state. The PL intensities of UP are both magnified by 50× for better visibility. The color scales represent the normalized intensity. The reflectivity dispersions in part a are directly translated to both parts b and c and show excellent agreement.
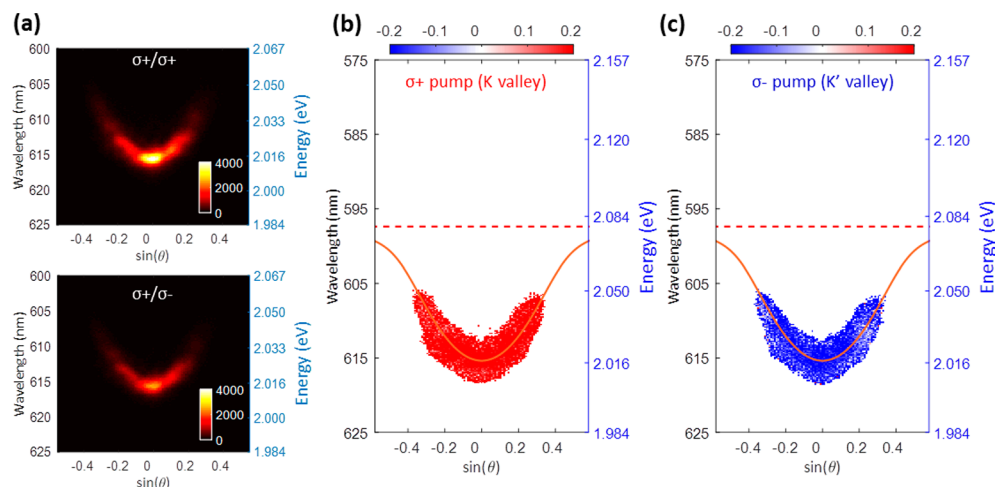
Figure 3. Observation of TPE valley-dependent helicity at 80 K. (a) Polarization-resolved k-space TPE fluorescence maps by 1045 nm pump with σ^+ polarization. As the pump is resonant with 2p dark states, TPE fluorescence maps detected at σ^+ (upper panel) and σ^- (lower panel) polarizations show prominent valley-dependent intensity contrast. (b) The TPE helicity map extracted from the σ^+ pump in part a. (c) The TPE helicity map with σ^- pump at 1045 nm. In both parts b and c, the orange solid lines represent the LP dispersion and the dashed lines represent ex$_A$. These two helicity maps show uniform helicities of about 20% but with opposite signs which are consistent with the pump polarizations.

induced LP (ground states) emission photons have strong intensity and follow $m_{ph}^{TPE}(\sim 2\omega) = m_{ph}^{pump}(\omega)$ (see Analysis). Since the intervalley scattering through the relaxation process cannot be neglected in the practical experiments, the optical spin m_{ph}^{TPE} reduces to an optical helicity less than unity as

$$\rho^{TPE} = \rho_{LP} \frac{1}{\left(1 + 2W_{K\leftrightarrow K'}^{2p}/W_{2p\rightarrow LP}\right)} \qquad (2)$$

where ρ_{LP} is the LP emission helicity at resonant excitation and $W_{K\leftrightarrow K'}^{2p}$ is the intervalley scattering at the 2p states (see Analysis).

SHG is a nonlinear process resulting from broken inversion symmetry in monolayer WS$_2$. When SHG is resonant with the

metastable UP state, the intensity is largely magnified by the UP resonance SHG process:[32,33]

$$I_{SHG} \propto W_{g_e \leftrightarrow UP}^{2ph(\omega)\rightarrow ph(2\omega)} \qquad (3)$$

By considering the 3-fold rotation symmetry and valley DOF in monolayer WS$_2$, the SHG emission photons show opposite spins with pump photons following $m_{ph}^{pump}(\omega) = -m_{ph}^{SHG}(2\omega)$ (see Analysis). In practical experiments, the SHG intensity and the emission optical spin depend on the comparisons between this SHG rate $W_{g_e \leftrightarrow UP}^{2ph(\omega)\rightarrow ph(2\omega)}$ and the UP decay rate ($W_{UP\rightarrow g_e}^{ph}$) (see Analysis).
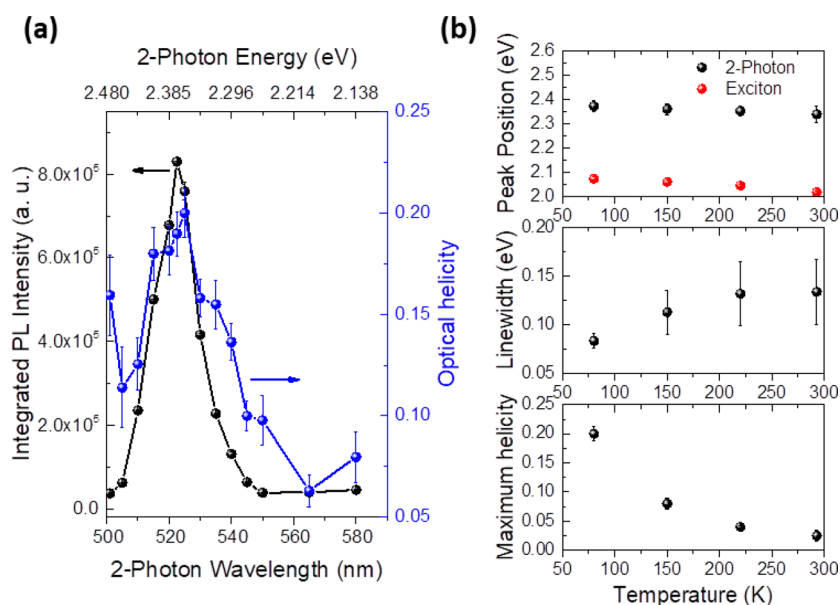
Figure 4. Revealing the TPE resonance of 2p states and its temperature dependence. (a) The integrated intensity (black) and maximum helicity (blue) as functions of the TPE pump wavelength. Both the intensity and the helicity peak at the effective two-photon wavelength around ∼522 nm, corresponding to the resonance of dark 2p states. (b) Temperature dependence of the TPE resonance peaks (upper panel), line width (middle panel), and maximum helicity (lower panel). The error bars for helicity are from multiple measurements, and those for line width and peaks, from peak fitting. As temperature increases, both the TPE resonance and control 1s exciton peaks show a similar trend of redshift as expected. Meanwhile, the line width gradually increases due to the stronger scattering process and faster relaxation dynamics, which is also the major reason for a decreasing helicity approaching zero.

For the observation of nonlinear optics, the strong coupling regime is first demonstrated in this monolayer WS$_2$ cavity and the corresponding EP photoluminescence (PL) is shown under different pump conditions. For clarity, the data in the main text are collected at 80 K unless otherwise stated (other temperatures (up to room temperature) are shown in the Supporting Information and Figure S5). To determine the strong coupling regime, k-space (angle-resolved) reflectivity mapping of white light is carried out as in Figure 2a. Two distinct anticrossing modes at the darker areas are clearly revealed and identified as the UP and LP. To confirm the formation of EPs, a coupled oscillator model is fitted with UP and LP as the solid gray and orange curves, respectively (see Analysis). A Rabi splitting of 41.6 meV and a large splitting to line width ratio of >3.3 are also obtained, in consistency with the previous report.[30] To observe the fluorescence, the EPs are first pumped by a pulsed laser of 560 nm, which lies on the edge of the cavity sideband. The ground-state LP is dominant, while the UP becomes visible as magnified by 50 times as in Figure 2b, suggesting a fast thermal relaxation from UP to LP. The PL dispersion also shows excellent agreement with the extracted reflectivity dispersion from Figure 2a. More importantly, the EPs could also be observed by TPE fluorescence (Figure 2c). The TPE can get access to the 2p dark states by pumping at 1045 nm, whose two-photon energy is close to the resonance of 2p states.[9,21,34] Remarkably, the TPE shows a prominent k-space fluorescence map, similar to the case of the linear pump at 560 nm. The LP is still dominant, while the UP is also magnified by 50 times for better visibility, and this dispersion is consistent with the reflectivity dispersion. This observation strongly suggests that the 2p resonance corresponds to one of the EP excited states, which inherits physical properties from the pure exciton constituent. Therefore, it may also imply that $W_{2p \to LP}$ happens via a direct

ultrafast interstate transition channel from 2p to lower optically allowed states and finally induced such prominent fluorescence from ground-state LP.

To look into the nonlinear optical response from the 2p excited states with this probable relaxation channel, the valley-polarized TPE induced fluorescence is performed. Here we focus on the ground-state (LP) emission polarization as an efficient indicator for the valley properties to infer the transition process.[22–24] When pumped with σ^+ (left circular) polarization at 1045 nm, the k-space fluorescence map is detected at both σ^+ and σ^- polarizations (Figure 3a). Clearly, the σ^+ TPE fluorescence has a much stronger intensity than the σ^- one, implying the inherited valley DOF.[9] To analyze the valley dependence, the measured TPE induced fluorescence helicity is defined as $\rho^{\mathrm{TPE}} = \frac{I(\sigma^+) - I(\sigma^-)}{I(\sigma^+) + I(\sigma^-)} \times 100\%$. A k-space helicity map in Figure 3b is extracted from Figure 3a, where a uniform valley helicity of about 20% is obtained along the LP band. When the pump is switched to the σ^- polarization, the TPE fluorescence contrast of σ^+ and σ^- is reversed and a k-space helicity map with about −20% helicity is obtained in Figure 3c. For comparison, the helicity maps with a linear pump at 560 nm only show optical helicity of about 8% (Figure S3).

As in eqs 1 and 2, the helicity from TPE, $\rho^{\mathrm{TPE}} = \rho_{\mathrm{LP}}(1 + 2W_{K \leftrightarrow K'}/W_{2p \to LP})^{-1}$, is determined by the term $W_{K \leftrightarrow K'}/W_{2p \to LP}$. For nonresonant excitation (e.g., the linear pump at 560 nm), the LP emission helicity has to follow the thermodynamic relaxation as $\rho = \rho_{\mathrm{LP}}(1 + 2W_{K \leftrightarrow K'}/W_{LP \to g_e})^{-1}$ with $W_{K \leftrightarrow K'} \propto \exp(\Delta E/k_B T)$, where $\Delta E = E_{\mathrm{pump}} - E_{\mathrm{LP}}$, E_{pump} is the pump energy, and E_{LP} is the LP energy (see Analysis).[24,29,35] The helicity of ρ_{LP} under resonant conditions is around 20%, as reported in a similar WS$_2$ cavity system by considering the pump conditions and polariton composi-
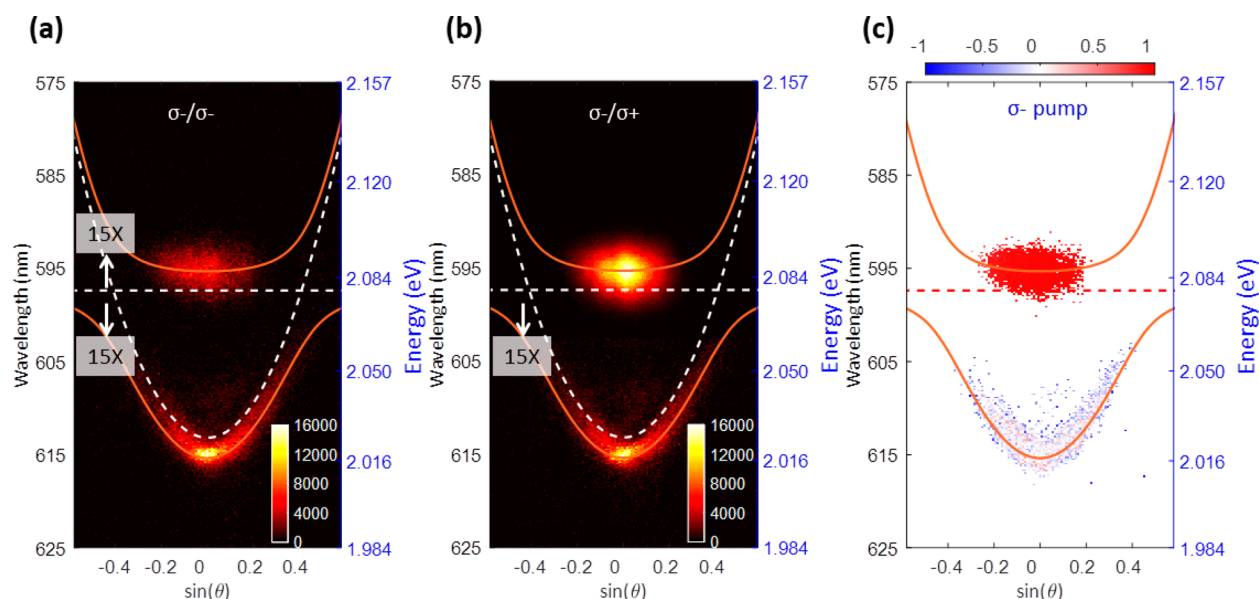
Figure 5. Probing the UP with valley DOF by resonant SHG. The k-space emission maps for (a) σ^- detection and (b) σ^+ detection when pumped with a 1190 nm laser with σ^- polarization. This pump is far off-resonance from the dark 2p state, and thus, the TPE is forbidden. There is still some leakage emission, as seen in LP of both parts a and b. For UP-resonant SHG, the k-space map surprisingly shows dominant SHG emission with opposite helicity in part b, while it only has negligible emission in part a. The dispersion curves are translated from Figure 2a, and the color bars represent the intensity. Note that the whole map in part a and LP in part b are magnified by 15 times for better visibility. (c) The helicity map extracted from parts a and b. The color bar represents the helicity. For the conservation of angular momentum with valley DOF, the UP shows a near-unity opposite helicity for resonant SHG. The LP has no apparent helicity for leakage emission.

tions.[25] In comparison with the LP energy ($\sim$2.016 eV), ΔE for the two-photon energy of the 1045 nm pump ($\sim$2.373 eV) is about 0.357 eV, while that for the 560 nm pump (2.214 eV) is about 0.198 eV. As a result, the TPE introduces unconventional relaxation that can surpass intervalley scattering ($W_{K\leftrightarrow K'} \propto \exp(\Delta E/k_B T)$ for observed helicity up to 20%, while the linear pump case follows the thermodynamic relaxation with a helicity of 8%. As the LP decay rate is estimated to be around 1 ps^{-1} [30] (see Analysis), the intervalley scattering rate $W_{K\leftrightarrow K'}$ for the linear pump at 560 nm is estimated to be around 0.75 ps^{-1}. This TPE maximum helicity is close to the resonant case ρ_{LP}, and this term $(1 + W^{2p}_{K\leftrightarrow K'}/W_{2p\rightarrow LP})^{-1}$ has to be near unity. Therefore, the TPE resonance with dark 2p states introduces an ultrafast relaxation channel ($W_{2p\rightarrow LP}$) from 2p states directly to LP with negligible intervalley scattering at 2p states, overcoming the thermalization limits in the linear excitation scheme. Note that this relaxation rate depends on the valley excitonic component[9] and refers to ultrafast dynamics of less than 500 fs, as reported for the intraexcitonic (2p−1s) transition.[36]

Notably, valley-polarized TPE spectroscopy is carried out to illustrate the resonance of 2p states. The excitation wavelength is scanned to two-photon energy close to UP. Both the TPE integrated fluorescence intensity and maximum helicity show apparent resonant peaks near the 1045 nm pump (i.e., two-photon energy at $\sim$522 nm) as in Figure 4a, unveiling the spectroscopic signature of this excited state. This resonance confirms this ultrafast channel from TPE is not governed by the thermalization relaxation through nonradiative decay but only related to the direct transition from 2p excited states to LP ground states. The terahertz optical transition is allowed between these two states;[5,6] thus, this direct transition from 2p to LP states may stem from terahertz transitions, following Fermi's golden rule with density of states for both 2p and LP states. The comprehensive picture of this direct valley-

dependent transition may deserve further dynamic investigations of terahertz photonics, but that is out of the scope of this work.

Moreover, similar TPE experiments at other temperatures up to RT are also carried out (see Figure S6). Figure 4b shows the temperature dependence of the resonance peak, line width, and maximum helicity. As temperature increases, both the TPE resonance and 1s exciton peak (control sample of isolated WS$_2$) positions show a similar trend of redshift, which is consistent with previous reports.[21,34] The line width gradually increases at higher temperature due to homogeneous broadening with a stronger scattering process and fast thermalization relaxation.[21,26] While these processes depolarize TPE fluorescence helicity to about zero at RT, the 2p intensity peak survives at RT. Though the temperature dependence may suggest the intervalley scattering $W^{2p}_{K\leftrightarrow K'}$ becomes significant at higher temperatures, it clarifies that the direct transitions from excited states 2p to EP are robust up to RT.

Meanwhile, we also observe unique UP-resonant SHG responses. UP is another typical excited state of EP lifted up by the Rabi splitting with much weaker emission than ground-state LP. As an example, the UP emission intensity around sin θ = 0 generally follows $I_{UP} \sim W^{ph}_{UP\rightarrow g_e} \times f(\exp[-(E_{UP} - E_{LP})/k_B T])$ (see Analysis), where $W^{ph}_{UP\rightarrow g_e}$ is the radiative decay rate of UP, and is estimated to be around 0.1 ps^{-1} based on the hybrid composition of excitons and photons;[30] $f(\exp[-(E_{UP} - E_{LP})/k_B T])$ is the function term of thermodynamic relaxation from UP to LP states; E_{UP} is the UP energy around sin θ = 0, and E_{LP} are the energies of available LP states. When pumped at 1190 nm, the TPE is far off-resonance from the 2p state and is thus forbidden. There is still weak leakage emission from forbidden excitation with extremely weak UP emission by detecting with the same polarization of pump as in Figure 5a.

However, when the emission is detected with the opposite polarization of pump, the UP shows brighter intensity by orders of magnitude around $\sin \theta = 0$, as in Figure 5b. The extracted helicity map for the σ^- pump in Figure 5c (vice versa for the σ^+ pump) shows a near unity opposite helicity for UP but close to zero helicity for LP. Due to the inversion symmetry breaking and the conservation of angular momentum as eq 3, this bright UP emission with opposite helicity is from the resonant SHG with a dominant rate of $W_{g_e \leftrightarrow \mathrm{UP}}^{2\mathrm{ph}(\omega) \rightarrow \mathrm{ph}(2\omega)}$. Therefore, the UP intensity follows $I_{\mathrm{UP}} \sim W_{g_e \leftrightarrow \mathrm{UP}}^{2\mathrm{ph}(\omega) \rightarrow \mathrm{ph}(2\omega)} \times f(\exp[-(E_{\mathrm{UP}} - E_{\mathrm{LP}})/k_{\mathrm{B}}T])$. By comparing these two cases, $W_{g_e \leftrightarrow \mathrm{UP}}^{2\mathrm{ph}(\omega) \rightarrow \mathrm{ph}(2\omega)}/W_{\mathrm{UP} \rightarrow g_e}^{\mathrm{ph}}$ is about 80, demonstrating UP-resonant SHG $W_{g_e \leftrightarrow \mathrm{UP}}^{2\mathrm{ph}(\omega) \rightarrow \mathrm{ph}(2\omega)}$ is an instantaneous process (<200 fs) dominating over the thermodynamic relaxation term of UP.[9,29,37] Moreover, the SHG resonances blueshift as the temperature increases up to 297 K without extinct helicity (see Figure S7), confirming that SHG is a dominating process over all other polariton thermodynamic relaxation at various temperatures. In consistency, we also observe a similar helicity dependence of LP-resonant pump SHG (see Figure S4). Thus, polariton-resonant SHG provides a universal approach to probe any states without thermodynamic influences.

In conclusion, the unique nonlinear optical responses from excited states of EP in a monolayer TMD are demonstrated via TPE and SHG spectroscopy. Based on the spectroscopic analysis and polarization dependence in these states, the transition process and valley dynamics in 2D EP are also resolved as unconventional new processes without thermodynamic relaxation limits in the linear optics. This study represents the first step toward the clear understanding of EP excited states and the underlying quantum electrodynamics and promises the feasibility of valley BEC and chiral superfluidity.[12,15] Moreover, the nonlinear optics and the underlying optical selection rule at EP excited states raise many possibilities in chiral terahertz photonics and coherent quantum manipulation of exciton polaritons[1,5,11] as well as nonlinear control in valleytronics.[9,15,29,37]

■ EXPERIMENTAL METHODS

Sample Preparation. The MC consists of a bottom DBR of 15.5 pairs of Nb_2O_5/SiO_2, a top DBR of 7.5 pairs of Si_3N_4/SiO_2, and a cavity composite layer, which includes an exfoliated monolayer WS_2, two sandwiching layers of HSQ, and a capping layer of Al_2O_3. A single-crystal silicon (100) wafer with deep etched markers (35 μm deep) is first precleaned by a Piranha solution. The bottom DBR is then deposited via ion beam sputtering (Veeco IBS) at a temperature of 120 °C with a pressure of $<5 \times 10^{-5}$ Torr. The sputtering rate is set to be ~ 0.1 nm/s to achieve ultrahigh flatness and $>99.95\%$ reflectivity with a center wavelength of 625 nm and stop bandwidth of ~ 200 nm. Since the monolayer WS_2 would be degraded at high temperature, the top DBR is fabricated by plasma enhanced chemical vapor deposition (PECVD) at a temperature of 350 °C.

The cavity layer structure is very crucial to maintain the high excitonic performance of monolayer WS_2. Here the monolayer WS_2 (2D Semiconductor, Inc.) is directly exfoliated onto a PDMS stamp and then transferred to DBR substrates. We have selected HSQ as the sandwiching layers to enhance the excitonic performance. The HSQ is first spin-coated onto the

substrate, and then, the spin-coated thin films are cross-linked into amorphous SiO_2 via thermal annealing at 400 °C in an Ar environment. The thicknesses for the bottom and top HSQ layers are controlled to be 105 and 90 nm, respectively. To prevent the damage from the plasma environment during the PECVD growth, another 5 nm of thermal Al_2O_3 is deposited onto the top HSQ layer by atomic layer deposition (ALD) at 200 °C. With the cavity layer structure design, the MC in this work forms a total $\lambda/2$ cavity with electric field distribution sharply peaked at the location of the WS_2 monolayer.

Optical Characterization. The k-space measurements are carried out in a home-built confocal setup attached with a spectrometer and a 2D EMCCD array camera (Andor spectrometer). This confocal setup is also integrated with a Janis open cycle cryostat (ST500) which can be cooled down to liquid helium temperature. The long working distance objective lens (NIKON Plan Fluor ELWD 40×) adapted in this work has a NA of 0.6 and objective correction collars for seeing through the cryostat window. The focused pump beam diameter with this objective is around 3 μm. The reflectivity is measured with a collimated white lamp source, while the PL, TPE, and SHG are all measured with a tunable pump laser. This tunable source consists of a tunable Ti:sapphire pulsed pump laser (Chameleon Ultra II, 690−1040 nm wavelength range, 80 MHz repetition rate, ∼200 fs pulse width), an optical parametric oscillator (OPO) that converts the pulse to a signal beam (1000−1360 nm), and SHG of the pump and OPO covers all of the visible wavelength range up 690 nm. There are two separate optical paths for the linear PL pump and the TPE/SHG pump. The linear PL is pumped by the laser OPO SHG port at 560 and 590 nm. The visible linear polarizer and half-wave plate are taken to control the linear polarization of PL excitation. The TPE/SHG is pumped by the laser OPO port with a wavelength range of 1000−1250 nm, and infrared (IR) optics is taken to control the linear polarization of nonlinear excitation. For the control of circular polarization, a broad-band Fresnel Rhomb quarter-wave retarder is used to cover all of the visible and IR ranges. The polarization control on the collection path is based on the visible linear polarizer and a half-wave plate.

■ ANALYSIS

Coupled Harmonic Oscillator Model. The polariton dispersion can be modeled using a coupled oscillator model[1,38]

$$\begin{pmatrix} E_{\mathrm{ex}} + i\hbar\Gamma_{\mathrm{ex}} & V_{\mathrm{A}} \\ V_{\mathrm{A}} & E_{\mathrm{cav}}(\theta) + i\hbar\Gamma_{\mathrm{cav}} \end{pmatrix} \begin{pmatrix} \alpha \\ \beta \end{pmatrix} = E \begin{pmatrix} \alpha \\ \beta \end{pmatrix}$$

Here the cavity mode was determined as $E_{\mathrm{cav}}(\theta) = E_{\mathrm{ph}}/\sqrt{1 - (\sin \theta/n_{\mathrm{eff}})^2}$ with E_{ph} being the cutoff photon energy and n_{eff} the reflective refractive index of the cavity layer. E_{ex} is the exciton energy. Γ_{cav} and Γ_{ex} are the half width at half-maximum (HWHM) of cavity photons and excitons, respectively. E are the eigenvalues corresponding to the energies of polariton modes. α and β construct the eigenvectors. V_{A} is the coupling strength. The eigenvalues are

$$E = \left(\frac{E_{\mathrm{ex}} + E_{\mathrm{cav}}}{2}\right) + i\left(\frac{\hbar\Gamma_{\mathrm{ex}} + \hbar\Gamma_{\mathrm{cav}}}{2}\right)$$
$$\pm \sqrt{V_{\mathrm{A}}^2 + \frac{1}{4}(E_{\mathrm{ex}} - E_{\mathrm{cav}} + i\hbar\Gamma_{\mathrm{ex}} - i\hbar\Gamma_{\mathrm{cav}})^2}$$

where $\hbar\Omega_{\text{Rabi}} = 2\sqrt{V_A^2 - \frac{1}{4}(\hbar\Gamma_{\text{ex}} - \hbar\Gamma_{\text{cav}})^2}$ is the Rabi splitting at detuning $\Delta E_{\text{cav}} - E_{\text{ex}} = 0$.

V_A^2 dominates in the square root part in this work, as analyzed in the main text. The splitting-to-line width ratio (SLR) can be represented as $\text{SLR} = \frac{\hbar\Omega_{\text{Rabi}}}{2\Gamma_{\text{polariton}}} \approx \frac{V_A}{\Gamma_{\text{polariton}}}$, where $\Gamma_{\text{polariton}}$ is the HWHM of polaritons. The interaction rate can be represented by V_A, and the polariton decay rate can be determined by the HWHM $\Gamma_{\text{polariton}}$; one can understand SLR as the ratio of the interaction rate to the polariton decay rate.

Note that α and β satisfying $|\alpha|^2 + |\beta|^2 = 1$ also represent the Hopfield coefficients of cavity photons and excitons for each polariton state as

$$|\alpha|^2 = \frac{1}{2}\left(1 + \frac{\Delta}{\sqrt{\Delta^2 + 4V_A^2}}\right)$$

$$|\beta|^2 = \frac{1}{2}\left(1 - \frac{\Delta}{\sqrt{\Delta^2 + 4V_A^2}}\right)$$

As a linear superposition of an exciton and a cavity photon, the decay rates of the polaritons are also determined by the Hopfield coefficients as

$$W_{\text{LP}} = |\alpha|^2 W_{\text{ex}} + |\beta|^2 W_{\text{cav}}$$

$$W_{\text{UP}} = |\beta|^2 W_{\text{ex}} + |\alpha|^2 W_{\text{cav}}$$

where W_{LP} and W_{UP} refer to the decay rates of lower polaritons (LPs) and upper polaritons (UPs), respectively, and W_{ex} and W_{cav} represent the decay rates of excitons and cavity photons, respectively.

Nonlinear Selection Rules of the Valley Polaritons. In the TPE induced LP fluorescence, the transition rate of two-photon excitation is[32,33]

$$W_{g_e \to f}^{2\text{ph}(\omega)} = \frac{2\pi e^4 \mathcal{E}^4}{\hbar\omega^4} \left| \sum_{i \neq f} \frac{\langle f|\epsilon\cdot\hat{\mathbf{p}}|i\rangle\langle i|\epsilon\cdot\hat{\mathbf{p}}|g_e\rangle}{E_i - \hbar\omega} \right|^2 \delta(E_f - 2\hbar\omega)$$

where $\mathcal{E}$ is the electric field amplitude, $\epsilon\cdot\hat{\mathbf{p}}$ is the transition dipole moment, g_e is the electronic ground state, i is the intermediate state for the nonlinear process, and f is the final state. When the final state f is the 2p state and resonant with two-photon energy $E_f = E_{2\text{p}} = 2\hbar\omega$, this rate could be largely enhanced. Therefore, the 2p state resonance can be directly depicted via TPE spectroscopy. Due to the 3-fold rotation symmetry of the hexagonal lattice in monolayer WS_2, the transition matrix elements $\langle f|\epsilon\cdot\hat{\mathbf{p}}|i\rangle$ and $\langle i|\epsilon\cdot\hat{\mathbf{p}}|g_e\rangle$ are required to remain unchanged under $\hat{C}_3$ in-plane rotation operation. It provides an intuitive picture that the overall out-of-plane angular momentum must conserve during the transition processes. For TPE of circularly polarized photons $\sigma^\pm$, angular-momentum conservation requires[32,33]

$$C_3(g_e) \pm 2m_{\text{ph}}^{\text{pump}}(\omega) = C_3(f) + 3N \qquad (N \text{ are integers})$$

where $C_3(g_e)$ and $C_3(f)$ are the angular-momentum quantum numbers in the electronic ground state and the final state, respectively, $\pm m_{\text{ph}}^{\text{pump}}$ represents the optical spins of pump photons $\sigma^\pm$, and $3N$ is the angular-momentum change from the crystal lattice with 3-fold symmetry.

The total angular momentum of the final excitonic state includes valley pseudospin angular momentum and exciton orbital angular momentum, as $C_3(f) = m_{\text{K(K')}} + m_l$. The angular momentum of the electronic ground state $C_3(g_e)$ is generally considered to be zero. For TPE resonant with the 2p state, $m_{\text{K}} = 1$ ($m_{\text{K'}} = -1$) and $m_l = \pm 1$. Therefore, for the TPE transition at a specific K(K') valley, the two photons have the same optical spins ($\sigma^\pm$) with the valley pseudospin $m_{\text{ph}}^{\text{pump}}(\omega) = m_{\text{K(K')}}$.[32,33]

TPE (resonance with the 2p state) induced LP fluorescence involves three processes: TPE from the electronic ground state g_e to the 2p excited state, an internal decay process from the optically dark 2p state to the bright LP state, and finally luminescence of one photon from the LP state to the ground state. The fluorescence intensity is given by[32,33]

$$I_{\text{TPE}} \propto W_{g \to 2\text{p}}^{2\text{ph}(\omega)} W_{2\text{p} \to \text{LP}} W_{\text{LP} \to g}^{\text{ph}(\sim 2\omega)}$$

Without considering the depolarization from the thermodynamic relaxation, the conservation of the overall angular momenta requires $2m_{\text{ph}}^{\text{pump}}(\omega) - m_{2\text{p} \to \text{LP}} - m_{\text{ph}}^{\text{TPE}}(\sim 2\omega) = 3N$ (N is an integer), where $m_{\text{ph}}^{\text{TPE}}(\sim 2\omega)$ is the spin angular momentum of TPE fluorescence photons and $m_{2\text{p} \to \text{LP}}$ is the change of total angular momentum during the ultrafast transition from 2p excitonic state to LP polariton state. Since the LP state is a coherent superposition of 1s excitonic state and cavity photon, the orbital angular momentum of LP is $m_{\text{LP}} = 0$, and thus, the total angular momentum is $m_{2\text{p} \to \text{LP}} = m_l = \pm 1$ under the condition of non-intervalley scattering. As a result, the TPE fluorescence photons preserve the helicity from pump photons with $m_{\text{ph}}^{\text{TPE}}(\sim 2\omega) = m_{\text{ph}}^{\text{pump}}(\omega) = m_{\text{K(K')}}$.[32,33]

SHG is an instantaneous process, where the initial and final states are considered as the same state g_e. And the intensity for resonant SHG with UP state follows[32,33]

$$I_{\text{SHG}} \propto W_{g_e \leftrightarrow \text{UP}}^{2\text{ph}(\omega) \to \text{ph}(2\omega)} = \frac{2\pi}{\hbar} |M_{g_e \leftrightarrow \text{UP}}|^2 \delta(E_{\text{UP}} - 2\hbar\omega)$$

where the transition matrix element of SHG is given by

$$M_{g_e \leftrightarrow \text{UP}} = \frac{e^3 \mathcal{E}_{2\omega} \mathcal{E}_\omega^2}{\omega^3} \frac{\langle g_e|\epsilon\cdot\hat{\mathbf{p}}|\text{UP}\rangle}{(E_{\text{UP}} - 2\hbar\omega + i\Gamma)} \sum_{i \neq \text{UP}} \frac{\langle \text{UP}|\epsilon\cdot\hat{\mathbf{p}}|i\rangle\langle i|\epsilon\cdot\hat{\mathbf{p}}|g_e\rangle}{E_i - \hbar\omega}$$

where $E_{2\omega}$ is the electric field amplitude of SHG photons and Γ is the line width of the emission state. The second term describes the SHG emission, and the last sum term describes the two-photon nonlinear process. Therefore, SHG intensity could be extremely strong and SHG demonstrates an ultrafast rate (instantaneous process) over the polariton dynamics when it is resonant with metastable UP states.

Without considering the ultrafast thermodynamic relaxation from the UP states, the conservation of angular momentum requires $C_3(g_e) + 2m_{\text{ph}}^{\text{pump}}(\omega) = C_3(f) + m_{\text{ph}}^{\text{SHG}}(2\omega) + 3N$. Since the initial and final states are the same g_e, it reduces to $2m_{\text{ph}}^{\text{pump}}(\omega) = -m_{\text{ph}}^{\text{SHG}}(2\omega) + 3N$. In this way, SHG emission photons always have the opposite helicity with the incident photons as $m_{\text{ph}}^{\text{SHG}}(2\omega) = -m_{\text{ph}}^{\text{pump}}(\omega)$.[32,33]

Dynamical Model of Excited-State Transitions with Valley Polarization. The valley polarization of TPE induced fluorescence can be modeled via rate equations. Here $n_{\text{K(K')}}^{2\text{p}}$ and $n_{\text{K(K')}}^{\text{LP}}$ denote the population of excitonic 2p states and

polaritonic LP states at $K(K')$ valley, respectively. The rate equations are written as[24,26,27]

$$\frac{dn_{K(K')}^{2p}}{dt} = P_{K(K')} - W_{2p\to LP}n_{K(K')}^{2p} - W_{K\leftrightarrow K'}^{2p}(n_{K(K')}^{2p} - n_{K'(K)}^{2p})$$

$$\frac{dn_{K(K')}^{LP}}{dt} = W_{2p\to LP}n_{K(K')}^{2p} - W_{K\leftrightarrow K'}^{LP}(n_{K(K')}^{LP} - n_{K'(K)}^{LP}) - W_{LP\to g_e}n_{K(K')}^{LP}$$

The first equation describes the dynamics of 2p states including optical pump with pumping rate $P_{K(K')}$ for each valley, 2p to LP decay process with a transition rate of $W_{2p\to LP}$, and 2p intervalley scattering processes with a scattering rate of $W_{K\leftrightarrow K'}^{2p}$. Since the 2p state is an optical dark state, the direct optical transitions from 2p to electronic ground state g_e are forbidden in the equation. The second equation describes the dynamics of LP states, including direct injections via 2p to LP decay channel, LP intervalley scattering with a scattering rate of $W_{K\leftrightarrow K'}^{LP}$, and LP polariton decay process with decay rate $W_{LP\to g_e}$.

The valley polarization of fluorescence induced by TPE is defined as $\rho^{TPE} = \frac{n_K^{LP} - n_{K'}^{LP}}{n_K^{LP} + n_{K'}^{LP}}$. For steady-state conditions, $\frac{dn_{K(K')}^{2p}}{dt} = \frac{dn_{K(K')}^{LP}}{dt} = 0$; thus, the valley polarization can be solved as

$$\rho^{TPE} = \frac{\rho_{LP}}{1 + \frac{2W_{K\leftrightarrow K'}^{2p}}{W_{2p\to LP}}}$$

where $\rho_{LP} = \frac{\rho_0}{1 + \frac{2W_{K\leftrightarrow K'}^{LP}}{W_{LP\to g_e}}} \approx \rho_0$ is the helicity of ground-state LP emission under resonant pump conditions, where $W_{K\leftrightarrow K'}^{LP}$ is negligible at low temperatures and ρ_0 is a proportionality constant depending on the pump conditions and the excitonic composition of polaritons.[25-27]

Our experimental observations can be understood by eq 2. The 2p states are excited and then undergo either intervalley scatterings or decay to LP states. If the transition rate $W_{2p\to LP}$ is much larger than the scattering rate $W_{K\leftrightarrow K'}^{2p}$, $\frac{W_{K\leftrightarrow K'}^{2p}}{W_{2p\to LP}} \approx 0$, ρ^{TPE} is preserved to be close to ρ_{LP}, as indicated by our experiments.

For the thermodynamic relaxation with nonresonant conditions, the rate equation is written as

$$\frac{dn_{K(K')}^{LP}}{dt} = P_{K(K')} - W_{K\leftrightarrow K'}(n_{K(K')}^{LP} - n_{K'(K)}^{LP}) - W_{LP\to g_e}n_{K(K')}^{LP}$$

where the intervalley scattering rate $W_{K\leftrightarrow K'} = W_0 \exp\left(\frac{E_{pump} - E_{LP} - \Delta}{k_BT}\right) \propto \exp\left(\frac{E_{pump} - E_{LP}}{k_BT}\right)$ is a function of the energy between the pump and LP states;[35] W_0 is the intervalley scattering when $E_{pump} - E_{LP} = \Delta$; Δ is the minimum activation energy for intervalley scattering.[35] The valley polarization with thermodynamic relaxation would then be solved as

$$\rho = \frac{\rho_0}{1 + \frac{2W_{K\leftrightarrow K'}}{W_{LP\to g_e}}}$$

The UP around $\sin(\theta) = 0$ generally has a much weaker emission intensity than the LP due to the radiative decay and thermodynamic relaxation and as follows

$$I_{UP} \sim W_{UP\to g_e}^{ph} \times f(\exp[-(E_{UP} - E_{LP})/k_BT])$$

where $W_{UP\to g_e}^{ph}$ is the radiative decay rate of UP, $f(\exp[-(E_{UP} - E_{LP})/k_BT])$ is the thermodynamic $\propto \sum_{LP} \exp[-(E_{UP} - E_{LP})/k_BT]$ relaxation from UP to all available LP states, E_{UP} is the UP energy around $\sin(\theta) = 0$, and E_{LP} are the energies of available LP states. If SHG is resonant with the UP states, this intensity becomes

$$I_{UP} \sim W_{g_e\leftrightarrow UP}^{2ph(\omega)\to ph(2\omega)} \times f(\exp[-(E_{UP} - E_{LP})/k_BT])$$

where the SHG rate $W_{g_e\leftrightarrow UP}^{2ph(\omega)\to ph(2\omega)}$ is as described in previous text.

■ ASSOCIATED CONTENT

ⓢ Supporting Information

The Supporting Information is available free of charge at https://pubs.acs.org/doi/10.1021/acs.nanolett.9b04811.

Sample characterizations, optical experimental setup, one-photon pump results, lower polariton-resonant SHG, temperature-dependent reflectivity and PL, temperature-dependent TPE, temperature-dependent SHG, and comparison with isolated monolayer (PDF)

■ AUTHOR INFORMATION

Corresponding Author

Xiang Zhang − Nanoscale Science and Engineering Center, University of California, Berkeley, Berkeley, California 94720, United States; Faculties of Sciences and Engineering, University of Hong Kong, Hong Kong, PR China; ⓞ orcid.org/0000-0002-3272-894X; Email: xiang@berkeley.edu

Authors

Xiaoze Liu − Nanoscale Science and Engineering Center, University of California, Berkeley, Berkeley, California 94720, United States; School of Physics and Technology, Wuhan University, Wuhan, Hubei 430072, PR China

Jun Yi − Nanoscale Science and Engineering Center, University of California, Berkeley, Berkeley, California 94720, United States; ⓞ orcid.org/0000-0003-2186-6615

Quanwei Li − Nanoscale Science and Engineering Center, University of California, Berkeley, Berkeley, California 94720, United States

Sui Yang − Nanoscale Science and Engineering Center, University of California, Berkeley, Berkeley, California 94720, United States

Wei Bao − Nanoscale Science and Engineering Center, University of California, Berkeley, Berkeley, California 94720, United States

Chad Ropp − Nanoscale Science and Engineering Center, University of California, Berkeley, Berkeley, California 94720, United States

Shoufeng Lan − Nanoscale Science and Engineering Center, University of California, Berkeley, Berkeley, California 94720, United States

Yuan Wang − *Nanoscale Science and Engineering Center, University of California, Berkeley, Berkeley, California 94720, United States*

Complete contact information is available at:
https://pubs.acs.org/10.1021/acs.nanolett.9b04811

Author Contributions

Notes

■ ACKNOWLEDGMENTS

■ REFERENCES

(1) Deng, H.; Haug, H.; Yamamoto, Y. Exciton-polariton Bose−Einstein condensation. *Rev. Mod. Phys.* **2010**, *82* (2), 1489−1537.

(2) Lodahl, P.; Mahmoodian, S.; Stobbe, S. Interfacing single photons and single quantum dots with photonic nanostructures. *Rev. Mod. Phys.* **2015**, *87* (2), 347−400.

(3) Coles, D. M.; Somaschi, N.; Michetti, P.; Clark, C.; Lagoudakis, P. G.; Savvidis, P. G.; Lidzey, D. G. Polariton-mediated energy transfer between organic dyes in a strongly coupled optical microcavity. *Nat. Mater.* **2014**, *13*, 712−719.

(4) Bose, R.; Cai, T.; Choudhury, K. R.; Solomon, G. S.; Waks, E. All-optical coherent control of vacuum Rabi oscillations. *Nat. Photonics* **2014**, *8*, 858−864.

(5) Ménard, J. M.; Poellmann, C.; Porer, M.; Leierseder, U.; Galopin, E.; Lemaître, A.; Amo, A.; Bloch, J.; Huber, R. Revealing the dark side of a bright exciton−polariton condensate. *Nat. Commun.* **2014**, *5*, 4648.

(6) Tomaino, J. L.; Jameson, A. D.; Lee, Y.-S.; Khitrova, G.; Gibbs, H. M.; Klettke, A. C.; Kira, M.; Koch, S. W. Terahertz Excitation of a Coherent L-Type Three-Level System of Exciton-Polariton Modes in a Quantum-Well Microcavity. *Phys. Rev. Lett.* **2012**, *108* (26), 267402.

(7) Dominici, L.; Colas, D.; Donati, S.; Restrepo Cuartas, J. P.; De Giorgi, M.; Ballarini, D.; Guirales, G.; López Carreño, J. C.; Bramati, A.; Gigli, G.; del Valle, E.; Laussy, F. P.; Sanvitto, D. Ultrafast Control and Rabi Oscillations of Polaritons. *Phys. Rev. Lett.* **2014**, *113* (22), 226401.

(8) Gibbs, H. M.; Khitrova, G.; Koch, S. W. Exciton−polariton light−semiconductor coupling effects. *Nat. Photonics* **2011**, *5*, 273.

(9) Xiao, J.; Ye, Z.; Wang, Y.; Zhu, H.; Wang, Y.; Zhang, X. Nonlinear optical selection rule based on valley-exciton locking in monolayer WS$_2$. *Light: Sci. Appl.* **2015**, *4*, No. e366.

(10) Rice, W. D.; Kono, J.; Zybell, S.; Winnerl, S.; Bhattacharyya, J.; Schneider, H.; Helm, M.; Ewers, B.; Chernikov, A.; Koch, M.; Chatterjee, S.; Khitrova, G.; Gibbs, H. M.; Schneebeli, L.;

Breddermann, B.; Kira, M.; Koch, S. W. Observation of Forbidden Exciton Transitions Mediated by Coulomb Interactions in Photoexcited Semiconductor Quantum Wells. *Phys. Rev. Lett.* **2013**, *110* (13), 137404.

(11) Sanvitto, D.; Kéna-Cohen, S. The road towards polaritonic devices. *Nat. Mater.* **2016**, *15*, 1061−1073.

(12) Schneider, C.; Glazov, M. M.; Korn, T.; Höfling, S.; Urbaszek, B. Two-dimensional semiconductors in the regime of strong light-matter coupling. *Nat. Commun.* **2018**, *9*, 2695.

(13) Barachati, F.; Fieramosca, A.; Hafezian, S.; Gu, J.; Chakraborty, B.; Ballarini, D.; Martinu, L.; Menon, V.; Sanvitto, D.; Kéna-Cohen, S. Interacting polariton fluids in a monolayer of tungsten disulfide. *Nat. Nanotechnol.* **2018**, *13* (10), 906−909.

(14) Vitanov, N. V.; Rangelov, A. A.; Shore, B. W.; Bergmann, K. Stimulated Raman adiabatic passage in physics, chemistry, and beyond. *Rev. Mod. Phys.* **2017**, *89* (1), 015006.

(15) Mak, K. F.; Shan, J. Photonics and optoelectronics of 2D semiconductor transition metal dichalcogenides. *Nat. Photonics* **2016**, *10*, 216−226.

(16) Dufferwiel, S.; Schwarz, S.; Withers, F.; Trichet, A. A. P.; Li, F.; Sich, M.; Del Pozo-Zamudio, O.; Clark, C.; Nalitov, A.; Solnyshkov, D. D.; Malpuech, G.; Novoselov, K. S.; Smith, J. M.; Skolnick, M. S.; Krizhanovskii, D. N.; Tartakovskii, A. I. Exciton−polaritons in van der Waals heterostructures embedded in tunable microcavities. *Nat. Commun.* **2015**, *6*, 8579.

(17) Liu, X.; Galfsky, T.; Sun, Z.; Xia, F.; Lin, E.-c.; Lee, Y.-H.; Kéna-Cohen, S.; Menon, V. M. Strong light−matter coupling in two-dimensional atomic crystals. *Nat. Photonics* **2015**, *9*, 30−34.

(18) Mak, K. F.; Lee, C.; Hone, J.; Shan, J.; Heinz, T. F. Atomically Thin MoS$_2$: A New Direct-Gap Semiconductor. *Phys. Rev. Lett.* **2010**, *105* (13), 136805.

(19) Splendiani, A.; Sun, L.; Zhang, Y.; Li, T.; Kim, J.; Chim, C.-Y.; Galli, G.; Wang, F. Emerging Photoluminescence in Monolayer MoS$_2$. *Nano Lett.* **2010**, *10* (4), 1271−1275.

(20) Chernikov, A.; Berkelbach, T. C.; Hill, H. M.; Rigosi, A.; Li, Y.; Aslan, O. B.; Reichman, D. R.; Hybertsen, M. S.; Heinz, T. F. Exciton Binding Energy and Nonhydrogenic Rydberg Series in Monolayer WS$_2$. *Phys. Rev. Lett.* **2014**, *113* (7), 076802.

(21) Ye, Z.; Cao, T.; O'Brien, K.; Zhu, H.; Yin, X.; Wang, Y.; Louie, S. G.; Zhang, X. Probing excitonic dark states in single-layer tungsten disulphide. *Nature* **2014**, *513*, 214−218.

(22) Cao, T.; Wang, G.; Han, W.; Ye, H.; Zhu, C.; Shi, J.; Niu, Q.; Tan, P.; Wang, E.; Liu, B.; Feng, J. Valley-selective circular dichroism of monolayer molybdenum disulphide. *Nat. Commun.* **2012**, *3*, 887.

(23) Zeng, H.; Dai, J.; Yao, W.; Xiao, D.; Cui, X. Valley polarization in MoS$_2$ monolayers by optical pumping. *Nat. Nanotechnol.* **2012**, *7*, 490−493.

(24) Mak, K. F.; He, K.; Shan, J.; Heinz, T. F. Control of valley polarization in monolayer MoS$_2$ by optical helicity. *Nat. Nanotechnol.* **2012**, *7*, 494−498.

(25) Sun, Z.; Gu, J.; Ghazaryan, A.; Shotan, Z.; Considine, C. R.; Dollar, M.; Chakraborty, B.; Liu, X.; Ghaemi, P.; Kéna-Cohen, S.; Menon, V. M. Optical control of room-temperature valley polaritons. *Nat. Photonics* **2017**, *11*, 491−496.

(26) Chen, Y.-J.; Cain, J. D.; Stanev, T. K.; Dravid, V. P.; Stern, N. P. Valley-polarized exciton−polaritons in a monolayer semiconductor. *Nat. Photonics* **2017**, *11*, 431−435.

(27) Dufferwiel, S.; Lyons, T. P.; Solnyshkov, D. D.; Trichet, A. A. P.; Withers, F.; Schwarz, S.; Malpuech, G.; Smith, J. M.; Novoselov, K. S.; Skolnick, M. S.; Krizhanovskii, D. N.; Tartakovskii, A. I. Valley-addressable polaritons in atomically thin semiconductors. *Nat. Photonics* **2017**, *11*, 497−501.

(28) Lundt, N.; Stoll, S.; Nagler, P.; Nalitov, A.; Klembt, S.; Betzold, S.; Goddard, J.; Frieling, E.; Kavokin, A. V.; Schüller, C.; Korn, T.; Höfling, S.; Schneider, C. Observation of macroscopic valley-polarized monolayer exciton-polaritons at room temperature. *Phys. Rev. B: Condens. Matter Mater. Phys.* **2017**, *96* (24), 241403.

(29) Wang, G.; Marie, X.; Gerber, I.; Amand, T.; Lagarde, D.; Bouet, L.; Vidal, M.; Balocchi, A.; Urbaszek, B. Giant Enhancement of the

Optical Second-Harmonic Emission of WSe$_2$ Monolayers by Laser Excitation at Exciton Resonances. *Phys. Rev. Lett.* **2015**, *114* (9), 097403.

(30) Liu, X.; Bao, W.; Li, Q.; Ropp, C.; Wang, Y.; Zhang, X. Control of Coherently Coupled Exciton Polaritons in Monolayer Tungsten Disulphide. *Phys. Rev. Lett.* **2017**, *119* (2), 027403.

(31) Wang, F.; Dukovic, G.; Brus, L. E.; Heinz, T. F. The Optical Resonances in Carbon Nanotubes Arise from Excitons. *Science* **2005**, *308* (5723), 838−841.

(32) Taghizadeh, A.; Pedersen, T. G. Nonlinear optical selection rules of excitons in monolayer transition metal dichalcogenides. *Phys. Rev. B: Condens. Matter Mater. Phys.* **2019**, *99* (23), 235433.

(33) Gong, P.; Yu, H.; Wang, Y.; Yao, W. Optical selection rules for excitonic Rydberg series in the massive Dirac cones of hexagonal two-dimensional materials. *Phys. Rev. B: Condens. Matter Mater. Phys.* **2017**, *95* (12), 125420.

(34) Zhu, B.; Chen, X.; Cui, X. Exciton Binding Energy of Monolayer WS$_2$. *Sci. Rep.* **2015**, *5*, 9218.

(35) Jin, C.; Ma, E. Y.; Karni, O.; Regan, E. C.; Wang, F.; Heinz, T. F. Ultrafast dynamics in van der Waals heterostructures. *Nat. Nanotechnol.* **2018**, *13* (11), 994−1003.

(36) Yong, C.-K.; Utama, M. I. B.; Ong, C. S.; Cao, T.; Regan, E. C.; Horng, J.; Shen, Y.; Cai, H.; Watanabe, K.; Taniguchi, T.; Tongay, S.; Deng, H.; Zettl, A.; Louie, S. G.; Wang, F. Valley-dependent exciton fine structure and Autler−Townes doublets from Berry phases in monolayer MoSe$_2$. *Nat. Mater.* **2019**, *18*, 1065−1070.

(37) Seyler, K. L.; Schaibley, J. R.; Gong, P.; Rivera, P.; Jones, A. M.; Wu, S.; Yan, J.; Mandrus, D. G.; Yao, W.; Xu, X. Electrical control of second-harmonic generation in a WSe$_2$ monolayer transistor. *Nat. Nanotechnol.* **2015**, *10*, 407−411.

(38) Savona, V.; Andreani, L. C.; Schwendimann, P.; Quattropani, A. Quantum well excitons in semiconductor microcavities: Unified treatment of weak and strong coupling regimes. *Solid State Commun.* **1995**, *93* (9), 733−739.